Modelling Secondary Break-Up of Melts in Sprays

Markus S., Fritsching U.

University of Bremen, SFB 372 "Spray Forming", Badgasteiner Straße 3, 28359 Bremen, Germany

Spray forming is a process to produce metals or metallic composites with improved material properties, which involves the disintegration of a molten material into droplets followed by their deposition on a substrate. The investigated melts were tin, copper and steel. The melt is atomised by means of a free-fall atomizer. To predict the resulting size distribution and solid fraction of the droplets in the spray a model was developed and tested in an uncoupled computation.

1. Introduction

In spray forming metallic melts are usually disintegrated by a free-fall atomizer. When the melt is poured out of the orifice, it falls due to gravity forces. During this stage it remains an unstable, but continuous jet. Then it breaks up into ligaments. Following to the stage of primary break-up, the ligaments and droplets break up into smaller droplets until the forces for further break-up recede. This disintegration process is combined to possible droplet coalescence during drop/drop impact. This multistage fragmentation process finally results in a spray droplet size distribution. The secondary break-up is generally defined as the fragmentation of ligaments into droplets, including the successive break-up of droplets into smaller droplets [1], [2]. In spray forming usually the melt mass flow (0.05 … 0.5 kg/s) is in order of the gas flow rate (0.08 … 0.5 kg/s). The gas to melt ratio is usually about 1 to 2 and the atomising zone is characterized by

- high acceleration of particles,
- high cooling rates and
- high particle bulk density.

Outgoing from a description of: the gas velocity field of the single phase flow, the break-up length of the molten jet, and an assumption for the distribution of primary break-up, a simple, two dimensional, uncoupled numerical computation of the atomised spray was developed. The most relevant process parameters as the gas to melt mass flow ratio GMR are taken into account. In the computation, every particle in the flow field (no particle parcels) is tracked by its acceleration, the effect of turbulence, the secondary break-up and the cooling of the molten droplet. Drop collision effects are neglected even though they are expected especially in the dense flow region.

The gas velocity field of the free-fall nozzle is characterised by individual supersonic jets of the secondary nozzle as illustrated in fig. 1. The jets of the primary gas are intended only to prevent some back flow. The region of the gas flow that is of interest for the atomisation is located inside the supersonic gas jets along the melt jet and it is subsonic. The gas flow field was investigated experimentally by LDA close to the secondary nozzle and more far away by Prandtl probe. At a nozzle distance more far away than 200 mm it was measured by a hot film probe (CTA). The turbulence intensity Tu at the centre is found to be constant at about 20%.

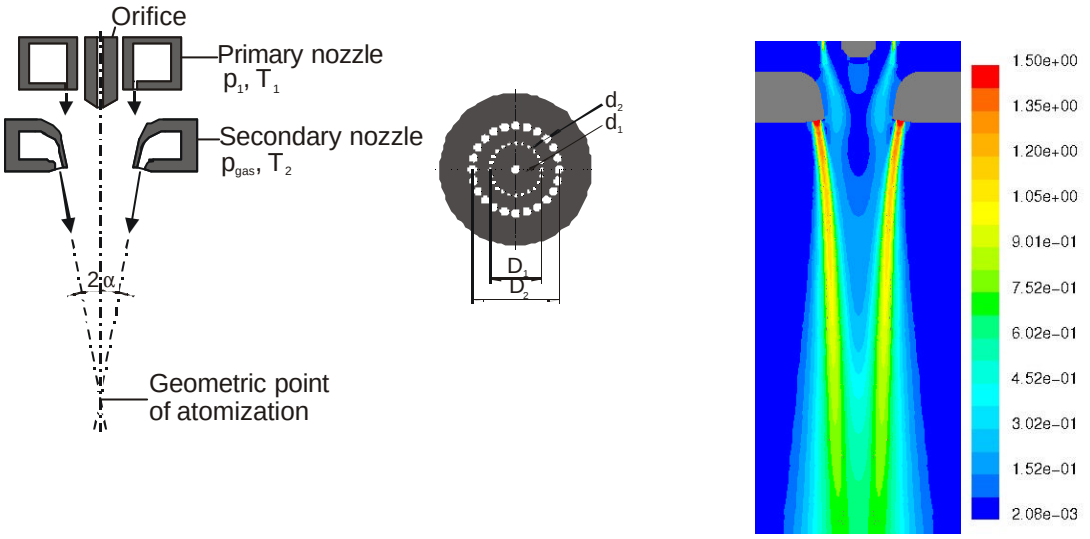

Fig. 1 Sketch of free-fall atomiser and contours of Mach number for the pd08 primary and sd02 secondary nozzle configuration for p_1 = 0.12 MPa and p_{gas} = 0.25 MPa

The mean gas velocity distribution along the melt jet axis can be described by a simple empirical function of the relative nozzle pressure p_{gas} and the nozzle distance from the nozzle x = 30 … 200 mm:

$$u_{gas}(x, r = 0) = f(x)\, p_{gas}^{\,g(x)} \text{ with}$$
$$f(x) = 40.479 - 2.261\, x + 0.0117\, x^2 - 0.0000178\, x^3$$
$$g(x) = 0.937 - 0.00638\, x + 0.000041898\, x^2 - 9.912\, 10^{-8}\, x^3$$

The break-up length ranges from $l_{breakup}$ = 10 … 55 mm depending on the material and nozzle pressure. The region of the primary break-up was investigated by means of high speed video [3]. In this region the local volume density may change drastically because of the jet instability of the melt when it pours out of the orifice. One obeys clusters of particle clouds in this region. Outgoing from linear stability analysis of the continuous melt jet [4], the mean initial ligament size may be estimated as d_{50} ~ 1 mm and the initial variance of the root normal distributed particles is estimated as σ_{var}^2 = 0.25, because the size distribution in the region of primary break-up was found to be very broad.

2. Modeling

2.2. Secondary Break-Up Of Molten Droplets

Droplet break-up mechanisms are classified mainly by the aerodynamic Weber number and the Ohnesorge number

$$We = \frac{\rho_{gas}\, u_{rel}^{\,2}\, d_{part}}{\sigma_{part}}, \quad Oh = \frac{\mu_{part}}{\sqrt{\rho_{part}\, d_{part}\, \sigma_{part}}}$$

in dependence of the relative velocity between the gas phase and the particle

$$u_{rel} = \left| \vec{u}_{gas} - \vec{u}_{part} \right|.$$

At moderate superheat for metallic melts the effect of viscosity is small. Different mechanisms of the break-up of molten metallic droplets were described by Krzeczkowski [5]. He distinguished between four break-up mechanisms: bag break-up for We = 12 … 20, umbrella break-up for We = 20 … 35, mixed break-up (of bag and umbrella type) for We = 35 … 70 and ligament break-up for We > 70. Below the limit of $We_{crit.}$ = 12 a droplet may still be deformed, but remain stable as one single droplet. A sketch of the bag and umbrella break-up is shown in figure 2.

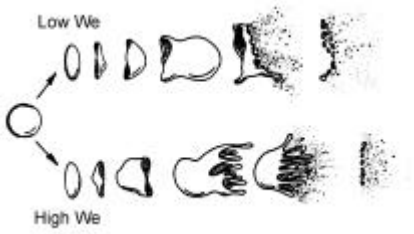

Fig. 2 Secondary break-up mechanism [6]

If one obeys the region of secondary break-up with high speed imaging, it was found especially for large particles with a diameter above 200 µm that the particles are not spherical, instead they have an irregular shape (fig. 3). It may be that these droplets are still in the state of deformation or break-up.

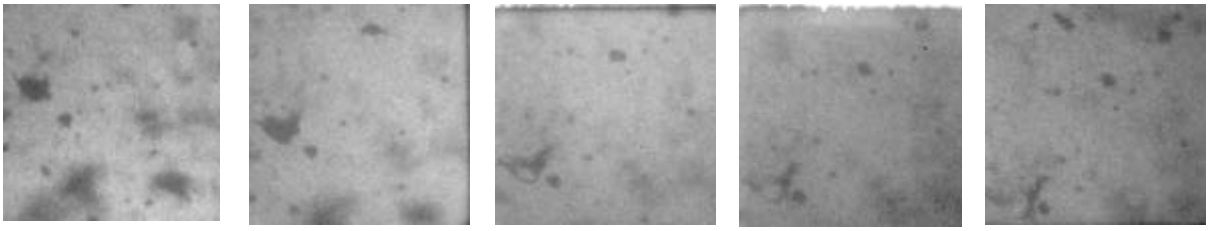

0 µs 20 µs 40 µs 50 µs 60 µs

Fig. 3 Bag break-up of a molten tin droplet of about 300 µm

Well known is the classification of Pilch and Erdmann [7], which includes a description of break-up mechanism for high Weber numbers above We > 350. For very small Weber numbers We < 12 a droplet may still break up into two equal sized droplets under certain conditions. According to this classification Samenfink et al. [8] distinguish between three mechanisms: bag break-up for We = 12 …. 20, multi mode break-up for We = 20 … 70 and shear break-up for We > 70.

The break-up dynamics is also depending on the aerodynamic Weber number. In a simplified model, the molten droplet deforms to a disk and then breaks up into new droplets (fig. 4). A characteristic break-up time t^* is defined as

$$t^* = \frac{d_{\mathrm{part}}}{u_{\mathrm{rel}}} \sqrt{\frac{\rho_{\mathrm{part}}}{\rho_{\mathrm{gas}}}} .$$

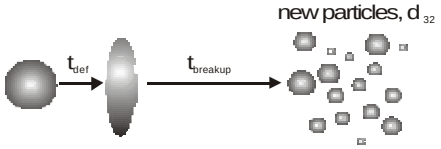

Fig. 4 Simplified model of break-up dynamics

The deformation time then is $t_{\mathrm{def}} = 1.6\ t^*$ due to Hsiang and Faeth [9]. The time needed for break-up is $t_{\mathrm{breakup}} = k\ t^*$, whereas k is an empirical constant depending on the break-up regime. The break-up time has been measured or estimated by Nigmatulin [10], Mayer [11] and Samenfink [8]. The latter made a comprehensive work about break-up regimes and break-up times. So his model is chosen here. Compared to the break-up time, the spheroidisation time is small, $t_{\mathrm{spheroidisation}} = 0.88\ m_{\mathrm{liquid}}\ d_{\mathrm{part}}/\sigma << t_{\mathrm{breakup}}$, [12]. For example, a molten steel 100 µm particle needs only about 250 ns to get spherical, that is many times faster than any possible break-up time. So it is assumed that new particles immediately after break-up are spherical.

From classification of droplet break-up mechanisms a model has been derived to describe the resultant droplet diameters after break-up. The TAB model of O'Rourke and

Amsden [13] results in a Sauter mean diameter d_{32} = 3/7 d_{part} for very low Weber numbers. The outgoing droplet diameter is d_{part}. For conventional liquids at various viscosities Hsiang & Faeth [9] found an empirical correlation between the Sauter mean diameter and the Ohnesorge and the Weber number.

$$d_{32} = 1.5\ \mathrm{Oh}^{0.2}\ \mathrm{We}^{-0.25}$$

Measured values for conventional liquids range from $\mathrm{Oh}^{0.2}\ \mathrm{We}^{-0.25}$ = 0.05 … 0.4. Metallic melts are also in this range. For shear break-up the new resultant droplet size is assumed to be root normal distributed around d_{50} = 1.2 d_{32} with a variance of σ_{var} = 0.238. This distribution was used respectively for the bag and multi mode break-up by Schmehl [14].

2.2. Acceleration of Particles

The acceleration of the particle is depending on the acting forces; that are mainly the drag force and the gravity force. The particle velocity is u_{part}.

$$m_{\text{part}} \frac{d\vec{u}_{\text{part}}}{dt} = \frac{1}{2} \rho_{\text{gas}} c_w \frac{\pi}{4} d_{\text{part}}^2 \left(\vec{u}_{\text{gas}} - \vec{u}_{\text{part}}\right) \left|\vec{u}_{\text{gas}} - \vec{u}_{\text{part}}\right| + m_{\text{part}} \vec{g}.$$

The gas velocity is divided in its mean and turbulent part.

$$\vec{u}_{\text{gas}} = \overline{\vec{u}_{\text{gas}}} + \vec{u}_{\text{gas}}'$$

For isotropic turbulence the velocity components of the turbulent part for all three spatial directions are normal distributed around the mean, the standard deviation σ_{var} is given by the turbulent kinetic energy k, σ_{var}^2 = 2/3 k. For the two-dimensional computation the resulting radial component of the turbulent velocity is corrected as

$$v_{\text{gas, res}}' = v_{\text{gas}}' + \left(\sqrt{\left(\frac{r}{\delta t}\right)^2 + w_{\text{gas}}'^2} - \frac{r}{\delta t}\right).$$

The radius is r and the time step is δt. During the lifetime of a turbulent vortex the corresponding turbulent gas velocity acts on a particle. The drag coefficient c_{w} of a spherical particle is depending on the Reynolds number.

$$\mathrm{Re} = \frac{\rho_{\text{gas}} u_{\text{rel}} d_{\text{part}}}{\mu_{\text{gas}}}$$

For *very* small particles the particles are forced to follow the gas flow. Considering the deformation of a molten droplet, Wiegand [15] estimates the drag coefficient of a liquid drop for low aerodynamic Weber numbers.

$$c_w = 0.28 + \frac{21}{\mathrm{Re}} + \frac{6}{\sqrt{\mathrm{Re}}} + \mathrm{We}_{\text{gas}} \left(-0.0042 \log^3(\mathrm{Re}) + 0.0471 \log^2(\mathrm{Re}) - 0.1579 \log(\mathrm{Re}) + 0.2319\right)$$

Schmehl [14] estimates the drag coefficient of the deforming drop increasing linear from 0.44 at t_0 up to 1.11 at t_{def}.

2.3. Cooling of Molten Particles

During its flight, a molten particle cools down rapidly. The rapid cooling an solidification of a molten particle undergoes at least four stages as shown for a simple alloy in figure 5. Within the first stage the particle cools down from superheat ΔT_{melt} above liquidus down to the

temperature $T_{nucleon}$ until first nuclei occur in the melt. A small particle may be undercooled about $\Delta T_{undercool}$ below $T_{liquidus}$. During the recalescence the temperature rises quickly. Then the particle solidifies further at an almost constant temperature until its completely solid. Finally the solid particle cools further down. It is assumed here, that the surface tension is suddenly increasing, if a molten particle solidifies. Hence no further break-up is possible.

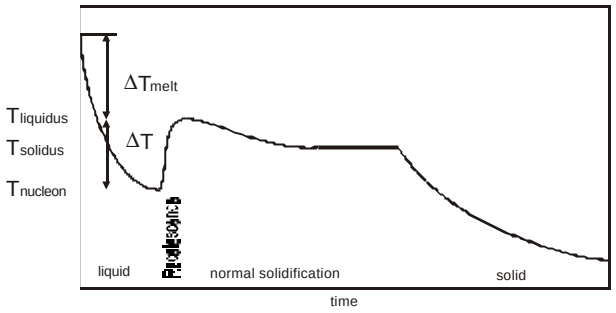

Fig. 5 Sketch curve of cooling for a metallic alloy

For molten particles at small Biot numbers, Bi = $\alpha\, d/\lambda << 1$, the temperature gradient inside the particle can be neglected. The assumption holds to be true here, because the particle diameters d are small and the heat conductivity λ for metallic melts has large values. The main part of the heat exchange between the particle and the gas is due to convection, a small part is due to radiation towards the spray chamber walls; for the liquid state see the following equation.

$$m_{part}\, c_p\, \frac{d\,T_{part}}{d\,t} = \pi\, d_{part}{}^2 \left(\alpha\,(T_{gas} - T_{part}) - \epsilon\,\sigma\left(T_{part}{}^4 - T_{wall}{}^4\right)\right)$$

The heat transfer coefficient α and hence the Nusselt number for a spherical particle is given by the Ranz-Marshall correlation; for a turbulent flow it should be corrected by the relative turbulence intensity κ.

$$\mathrm{Nu} = \frac{\alpha\, d_{part}}{\lambda_{gas}} = 2 + 0.6\,\mathrm{Re}^{\frac{1}{2}}\,\mathrm{Pr}^{\frac{1}{3}}\left(1 + 3.4\,\kappa^{0.843}\right),\quad \kappa = \frac{1}{\left|\vec{u}_{gas} - \vec{u}_{part}\right|}\sqrt{\frac{2}{3}k}$$

By an estimation of first nucleation at $T_{nucleon}$ temperature of a molten particle can be computed iteratively by finding the root of the following simplified equation.

$$\Delta T_{undercool+1} = \sqrt{\frac{M\, T_{liquidus}\, \Delta h_f}{e^{14214.64\, V_{part}}\, k\, N_{atom}\, T_{nucleon}}\,\frac{1.526814}{\log\left(\frac{\Delta T_{undercool}}{1.909859}\,\frac{10^{41}\, m^{-3}\, s^{-2}\, V_{part}\, e^{7107.320\, V_{part}}}{\dot{r}}\right)}}$$

$$T_{nucleon} = T_{liquidus} - \Delta T_{undercool}$$

where $V_{part} = \pi/6\ d_{part}{}^3$ is the volume of one particle, M is the molar mass, N_{atom} is the Avogadro constant and k is the Boltzmann constant. For further cooling and solidification modelling see Bergmann [16].

2.4. Computation

The computational domain is a 2-dimensional structured grid of 50 x 200 nodes. The computation so far is uncoupled (particles will have no effect on the gas phase). The field variables are the mean velocity u_{gas}, v_{gas}, the kinetic energy k, and the gas temperature T_{gas}. The turbulent components u'_{gas}, v'_{gas} are derived from random numbers. *Each* particle will be calculated. The time step size was dt = 10 µs and 10000 iterations have been calculated for each case. About 10^6 Particles are tracked every time step.

The melt jet is poured out of an orifice of 4 mm in diameter and the initial jet velocity is about 2.2 m/s. It is assumed that the molten jet pours out with its original melting temperature T_{melt} from the tundish. The atomising gas is nitrogen N_2. The process parameters and the physical fluid properties of the atomised metals are listed in table 1.

Table 1 Physical properties of melts

Material			Sn	Cu	Steel
Mass flow rate	m	[kg/s]	0.177	0.21	0.19
Temperature of the melt	T_{melt}	[°C]	257	1383	1661.7
Temperature at liquidus	$T_{liquidus}$	[°C]	232	1083	1511.7
Temperature at solidus	T_{solid}	[°C]	232	1083	1467.4
Density	r_{liquid}	[kg/m³]	7000	8000	6995
Viscosity	m_{liquid}	[kg/m s]	0.00185	0.004	0.0052
Surface tension	s	[N/m]	0.54	1.285	1.825
Heat capacity at liquidus	$c_{p,\ liquidus}$	[J/kg K]	250	619.7	840
Heat capacity at liquidus	$c_{p,\ solidus}$	[J/kg K]	226	435.9	720
Heat of fusion	Δh_f	[J/kg]	55600	213500	276500

3. Results

Most particles will be produced in a short distance behind the region of the primary break-up. Then the droplets are accelerated and spread out due to turbulence. Figure 6 shows a typical distribution of the droplets.

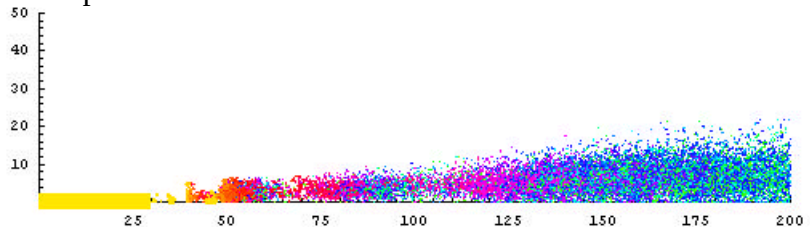

Fig. 6 Particle distribution for a spray cone atomised at 0.4 MPa

The basic influence of the increased GMR and hence the nozzle pressure will be discussed by an example: A steel jet at 150 °C superheat is atomised with nitrogen. The resulting particle distribution is shifted from big to small particles for increasing the nozzle distance, see fig. 7. Especially in the beginning of the disintegration process only a few large droplets or ligaments contain most of the total mass. The number distribution is *not* favourable for a description of the spray cone in spray forming as for the compaction the heat and mass flux is desired. If one looks only at the number distribution, changes in the size distribution of the spray cone are hardly recognized.

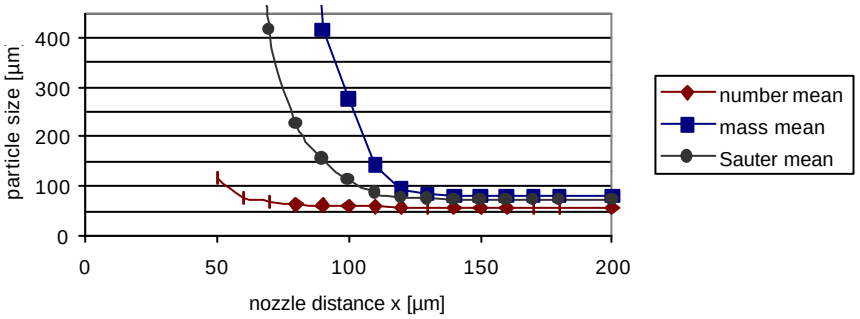

Fig. 7 Number, mass and Sauter mean diameter along the nozzle distance atomised at 0.4 MPa

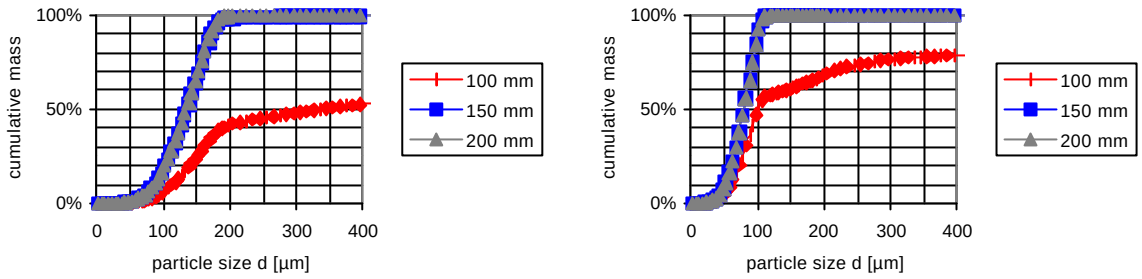

Fig. 8 Size distribution at the distance x of the gas nozzle of an atomised steel jet, relative nozzle pressure p_{gas} = 0.25 MPa (left) and p_{gas} = 0.4 MPa (right)

If one compares the particle distribution for two different nozzle pressures p_{gas}, a finer median particle size for higher pressure is found (fig. 8). At the distance of 100 mm below the gas nozzle there is still an amount of particles larger than 400 µm containing up to almost 50% of the total mass. For distances above 150 mm the atomised droplets reach their final distribution. For the radial distribution it may be shown that particles far away from the middle of the spray cone are smaller than at the spray cone centre (fig. 12).

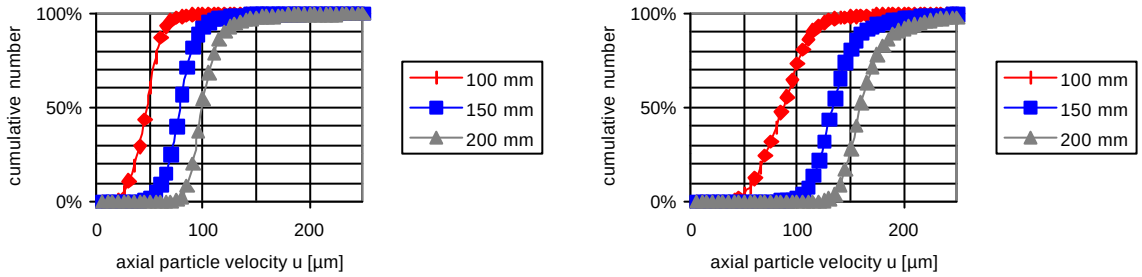

Fig. 9 Distribution of the axial particle velocity u at the distance x of the gas nozzle of an atomised steel jet, relative nozzle pressure p_{gas} = 0.25 MPa (left) and p_{gas} = 0.4 MPa (right)

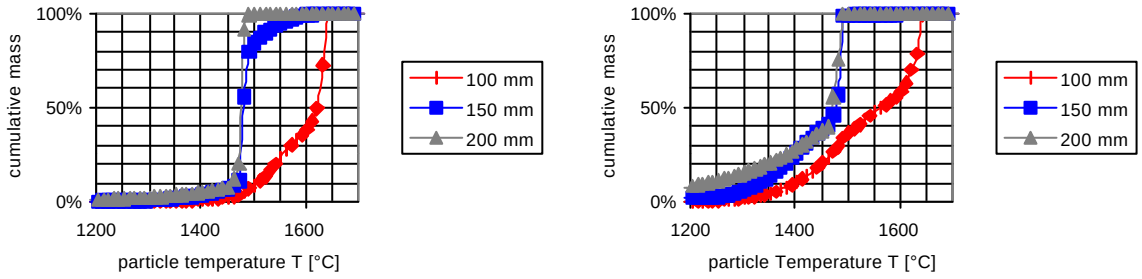

Fig. 10 Distribution of the particle temperature T_p at the distance x of the gas nozzle of an atomised steel jet, relative nozzle pressure p_{gas} = 0.25 MPa (left) and p_{gas} = 0.4 MPa (right)

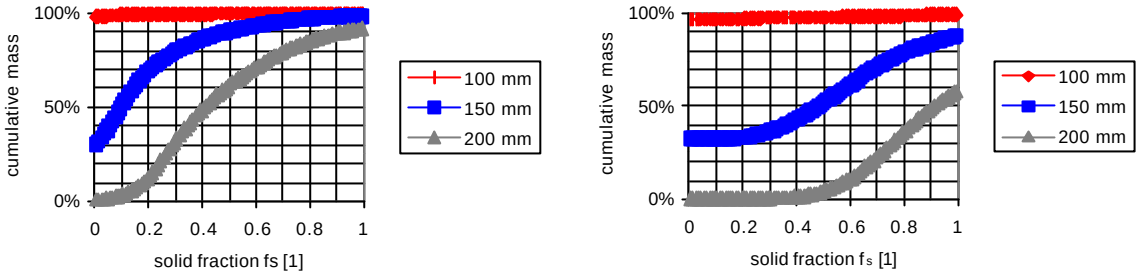

Fig. 11 Distribution of the solid fraction f_s at the distance x of the gas nozzle of an atomised steel jet, relative nozzle pressure p_{gas} = 0.25 MPa (left) and p_{gas} = 0.4 MPa (right)

The mean particle velocity for every particle size class is increasing along the distance and with an increased nozzle pressure (fig. 9). If one obeys the number average of the axial particle velocity it is also found that it increases for each particle size class along the distance. Especially small particles will be accelerated almost up to the gas velocity.

For a higher nozzle pressure the particles will cool down faster, so a larger amount of the total mass will be shifted to lower temperatures (fig. 10). Most of the particles will stay at the transformation temperature; above they are completely liquid as shown in fig. 4. At a distance of 100 mm below the gas nozzle almost all of the mass is still liquid. At a distance of 200 mm depending on the cooling quite an amount of mass will be partially solidified (semisolid). The area below the curve in figure 11 shows the total amount of liquid fraction. As the cooling rate is depending on the particle size a smaller amount of liquid fraction remains by an increased nozzle pressure. The same trends for the particle size, velocity (and temperature) distribution are measured by particle measurements methods like PDA and high speed pyrometer.

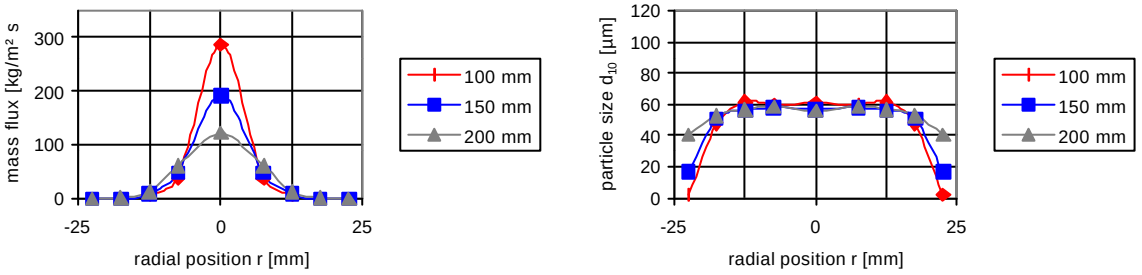

Fig. 12 Mass flux density and particle size along the radial position for different distances beneath the atomizer nozzle, relative nozzle pressure p_{gas} = 0.25 MPa (left) and p_{gas} = 0.4 MPa (right)

The radial mass flux density distribution inside the spray cone has a Gaussian shape and the spray cone spreads out for an increasing distance from the nozzle as shown in figure 12 for a nozzle pressure of 0.25 MPa. The mass flux distribution in the near field seems to be only slightly affected by an increased nozzle pressure, the distribution for a higher pressure (0.4 MPa not shown here) looks similar, while for the far field the maximum in the middle is reasonably increasing with an increasing nozzle pressure. Anyway the maximum values are a too low compared to the values predicted by the spray cone spreading outgoing from experiments in the far field. The radial distribution in the near field is mainly affected by the turbulence of the flow. It is described by the characteristic length scale L_T of the vortices.

If one compares the influence of different material properties on the droplet size distribution, the main influence is found for the surface tension. A lower surface tension will result in a finer droplet distribution.

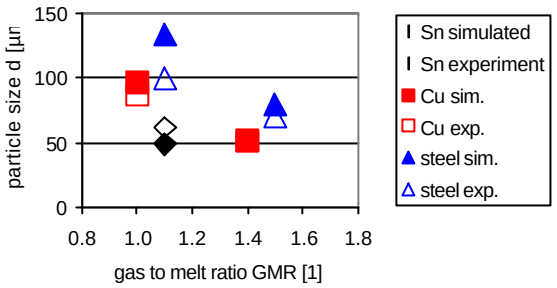

Fig. 13 Comparison of the simulated and experimental mass median diameter $d_{50,3}$ for different materials in dependency of the gas to melt ratio GMR

To check the quality of the simulated results, they are compared to the mass median diameter from experiments under identical conditions (fig. 13). The mass median diameter of a bulk of particles was measured by sieving analysis, which is most reliable under the ambiguous process conditions in spray forming. The error of the simulated $d_{50,3}$ lies in between 20% of the measured values except for the case of steel at GMR = 1.1, where the error is 34%. It should be pointed out that the estimated error of the measured values is also about 5%.

An interesting observation is, that the time needed for a melt droplet to break-up in a typical atomiser flow field, in some cases (if the superheat is low and the initial droplet size distribution is fine), may be longer than the time needed to freeze it. This could explain the difficulty of making finer gas atomised metal powders by using higher pressures and higher gas/metal ratios, as these will both accelerate cooling.

4. Summary and Conclusion

Especially in spray forming the large particles in the spray carry most of the mass and hence the thermal energy which comes from the melt flow. Even though these large particles are small in number they will determine the thermal state of all further disintegrated particles. And this is one of the key parameters to insure a good spray compaction on the deposit surface. Trying to understand the combination of particle acceleration, droplet break-up and collision and cooling of the liquid phase at an early stage in the spraymay lead to a better prediction for setting the appropriate process parameters in order to achieve better material properties of the sprayed deposit or powder.

5. Acknowledgement

The author gratefully acknowledges the support of the Deutsche Forschungsgemeinschaft (DFG) within the Sonderforschungsbereich 372 “Spray Forming” at the University of Bremen, Germany.

6. References

[1] Dombrowski N, Johns W R 1963 *The aerodynamic instability and disintegration of viscous liquid sheets, Chem. Eng. Sci.* **18** 203 – 214

[2] Klar E, Fesko J W 1984 *Powder Metallurgy Metals Handbook, Vol. 7* (9th edn; American Society for Metals, Materials Park, Ohio)

[3] Markus S, Fritsching U, Bauckhage K 2002 *Jet break up of liquid metal in twin fluid atomistion, Materials Science and Engineering* **A326** 122 – 133

[4] Markus S, Fritsching U 2002 *Instability Processes in Melt Atomization, Proc. of Powder Mettallurgy & Particultae Materials, June 16-21*, **3** 137 - 149
[5] Kreczkowski S A *International Journal of Multiphase Flow* **6** 227
[6] Yule A J, Dunkley J J 1994 *Atomization of Melts For Powder Production and Spray Deposition* (Oxford Series on Advanced Manufacturing II)
[7] Pilch M, Erdmann C A 1987 *Use Of Breakup Time Data And Velocity History Data To Predict The Maximum Size Of Stable Fragments For Accelaration-Induced Breakup Of A Liquid Drop*, *Int. Journal of Multiphase Flow, Vol. 13* **6** 741-757
[8] Samenfink W, Elsäßer A, Dullenkopf K et al. 1994 *Secondary Breakup of Liquid Droplets: Experimental Investigation for A Nummerical Descriptiom.* Proceedings ICLASS-94 156-163
[9] Hsiang L-P, Faeth G M 1992 *Near-Limit Drop Deformation and Secondary Breakup. International Journal of Multiphase Flow* **18(5)** 635-652
[10] Nigmatulin R I 1990 *Dynamics of Multiphase Media* English Edition Editor Vol. 1,2
[11] Mayer W O 1993 *Zur koaxilen Flüssigkeitszerstäubung im Hinblick auf die Treibstoff-aufbereitung in Raketentriebwerken* Dissertation Universität Erlangen
[12] Nichioorenko O S, Naida Yu I 1968 *Soviet Powder Metallurgy Metal Ceramics* **67** 509
[13] O'Rourke P J, Amsden A A 1987 *The TAB Method For Numerical Calculation Of Spray Droplet Breakup*, *Los Alamos National Laboratory* LA-UR-87-2105
[14] Schmehl R 2000 *CFD Analysis of Fuel Atomization, Secondary Droplet Breakup and Spray Dispersion in the Premix Duct of a LPP Combustor, 8. Int. Conference on Liquid Atomization and Spray Systems, Passadena, CA, USA, July 2000*
[15] Wiegand H 1987 *Die Einwirkung eines ebenen Strömungsfeldes auf frei bewegliche Tropfen und ihren Widerstandsbeiwert im Reynoldszahlbereich von 50 bis 2000* Fortschr.-Ber. VDI Reihe 7, Nr. 120, VDI-Verlag, Düsseldorf
[16] Bergmann D, Fritsching U, Bauckhage K 2000 *A mathematical model for cooling and rapid solidification of molten droplets, Int. J. Therm Sci.* **39** 53 - 62